

Significant enhancement of upper critical fields by doping and strain in iron-based superconductorsC. Tarantini,^{1,*} A. Gurevich,² J. Jaroszynski,¹ F. Balakirev,³ E. Bellingeri,⁴ I. Pallecchi,⁴ C. Ferdeghini,⁴ B. Shen,⁵ H. H. Wen,⁵ and D. C. Larbalestier¹¹*Applied Superconductivity Center, National High Magnetic Field Laboratory, Florida State University, 2031 E. Paul Dirac Drive, Tallahassee, Florida 32310, USA*²*Department of Physics, Old Dominion University, Norfolk, Virginia 23529, USA*³*National High Magnetic Field Laboratory, Los Alamos National Laboratory, Los Alamos, New Mexico 87545, USA*⁴*CNR-SPIN, Corso Perrone 24, 16152 Genova, Italy*⁵*Institute of Physics, Chinese Academy of Sciences, Beijing, China*

(Received 17 October 2011; revised manuscript received 20 October 2011; published 17 November 2011)

We report measurements up to 85 Tesla of the upper critical fields $H_{c2}(T)$ on $\text{Ba}_{1-x}\text{K}_x\text{As}_2\text{Fe}_2$ single crystals and $\text{FeSe}_{1-x}\text{Te}_x$ films tuned by doping and strain. We observed an H_{c2} enhancement by more than 25 T at low temperatures for the optimally doped $\text{Ba}_{1-x}\text{K}_x\text{As}_2\text{Fe}_2$ as compared to the previous measurements and extraordinarily high slopes of $dH_{c2}/dT = 250\text{--}500$ T/K near T_c in $\text{FeSe}_{1-x}\text{Te}_x$, indicating almost-complete suppression of orbital pair breaking. Theoretical analysis of $H_{c2}(T)$ suggests an inhomogeneous Fulde-Ferrel-Larkin-Ovchinnikov state below 10K for $H//ab$ in the optimally doped $\text{Ba}_{1-x}\text{K}_x\text{As}_2\text{Fe}_2$ and below 3K for $H//c$ and 9K for $H//ab$ in $\text{FeSe}_{1-x}\text{Te}_x$. The analysis also shows that H_{c2} in a multiband Fe-based superconductor can be significantly enhanced by doping and strain by shrinking and expanding different pockets of the Fermi surface, which can be more effective than the conventional way of increasing H_{c2} by nonmagnetic impurities.

DOI: [10.1103/PhysRevB.84.184522](https://doi.org/10.1103/PhysRevB.84.184522)

PACS number(s): 74.70.Xa, 74.20.Mn, 74.25.Op

I. INTRODUCTION

The discovery of the diverse family of Fe-based superconductors¹ (FBSs) in which an interplay of superconductivity and magnetism in layered semimetals can result in transition temperatures $T_c \leq 55\text{K}$ ^{2,3} has caused great interest. FBSs also have extremely high and only moderately anisotropic upper critical fields $H_{c2}(T)$, which often significantly exceed the paramagnetic limit B_p [T] = $1.84T_c$ [K] at which the Zeeman depairing energy is greater than the binding energy of the Cooper pairs.^{4–11} As a result, FBSs may exhibit exotic effects at high magnetic fields, in particular, paramagnetic pair breaking for multiband pairing,¹² and the inhomogeneous Fulde-Ferrel-Larkin-Ovchinnikov (FFLO) state.^{13–15}

The small Cooper pair sizes $\xi_0 = 1\text{--}3$ nm of FBSs indicate that the usual way of increasing H_{c2} —by introducing disorder in the dirty limit $\ell < \xi_0$ ¹⁶—can hardly work in FBSs, as it would require an elastic mean free path ℓ close to the lattice spacing. However, the low Fermi energies and multiband electronic structure of FBSs offer a new opportunity for tuning H_{c2} by shifting the Fermi level through expansion or contraction of different electron and hole pockets of the Fermi surface (FS), which also facilitates the FFLO transition.¹² This feature is amplified by a doping-induced Lifshitz transition caused by the emergence of small FS pockets from bands just below the Fermi level.¹² Such FS pockets have been revealed by *ab initio* calculations and angle-resolved photoemission spectroscopy (ARPES),^{2,17–20} particularly for $\text{FeSe}_{1-x}\text{Te}_x$, which has rather small Fermi energies of $E_F = 20\text{--}50$ meV. In this case, the increase of H_{c2} is not a mere consequence of the dependence of T_c on doping, because the shape of $H_{c2}(T)$ also changes significantly due to interplay of orbital and paramagnetic pair breaking in different bands. In this paper, we provide the first experimental evidence for the significant enhancement of H_{c2} in the optimally doped $\text{Ba}_{1-x}\text{K}_x\text{As}_2\text{Fe}_2$ (Ba-122) below 30K using high-field measurements up to 85 tesla (T), which

extend well beyond the previous measurements of H_{c2} on $\text{Ba}_{1-x}\text{K}_x\text{As}_2\text{Fe}_2$ ^{4,7,21} and $\text{FeSe}_{1-x}\text{Te}_x$.^{8,9}

II. MEASUREMENTS

We studied three $\text{Ba}_{1-x}\text{K}_x\text{Fe}_2\text{As}_2$ crystals grown by the flux method,^{22,23} one optimally doped with $x = 0.4$ (Ba-1) and two underdoped ones with $x = 0.25$ (Ba-2) and 0.15 (Ba-3). The samples had resistive transition midpoints at $T_c = 38.4\text{K}$, 28.2K , and 11.7K with transition widths at $\Delta T_c = 1\text{K}$, 1.1K , and 2.6K , respectively. $\text{FeSe}_{0.5}\text{Te}_{0.5}$ films were grown by pulsed laser deposition from a target with $T_c = 16.2\text{K}$. Several *c*-axis and in-plane-oriented films with thickness from 100 to 400 nm and 2×5 mm² sizes in the *ab* plane were grown on single-crystal $\text{LaAlO}_3(001)$ substrates in high vacuum at 550°C . The films have $T_c = 17.5\text{K}\text{--}18.9\text{K}$, and $\Delta T_c = 0.8\text{K}\text{--}1.3\text{K}$. These films were characterized in Refs. 24 and 25, where the enhancement of T_c by strains was related to the distortions of the (Se,Te)–Fe–(Se,Te) bond angle and length.

Magnetotransport measurements of the resistance $R(H)$ at low fields were performed in a 9-T physical property measurement system (Quantum Design), while high-field measurements were done within the 45-T hybrid direct current (DC) magnet and the 60- and 85-T pulsed magnets at the National High Magnetic Field Laboratory in Tallahassee, Florida, and Los Alamos, New Mexico. To minimize heating in pulsed fields, $\text{Ba}_{1-x}\text{K}_x\text{Fe}_2\text{As}_2$ crystals were cleaved down to $2 \times 0.3 \times 0.1$ mm³. A 100-kHz alternating current was employed, and the data were analyzed using a low-noise digital lock-in technique. Since the heating effect is usually more pronounced at lower temperatures and with the field perpendicular to the largest sample surface, we verified that the up- and down-field sweeps in such conditions for Ba-2 do not result in noticeable hysteresis in the $R(H)$ curves, as shown in Fig. 1. The almost-identical transition position and the absence of any low-field tail in $R(H)$ in the down

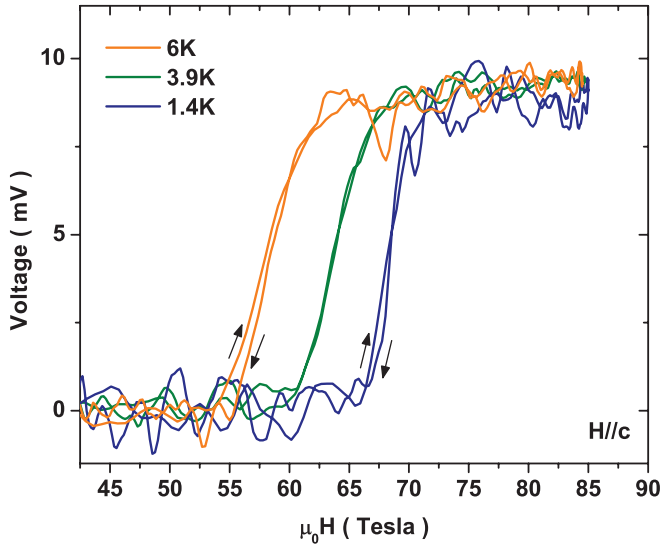


FIG. 1. (Color online) Superconducting transitions for Ba-2 measured in the 85-T pulsed magnet for $H//c$ showing both up- and down-field sweeps.

sweeps are indicative of negligible heating effects. The sample resistance $R(T, H)$ was measured for fields both parallel and perpendicular to the ab planes in order to determine $H_{c2}^{||}(T)$ and $H_{c2}^{\perp}(T)$, respectively, and $H_{c2}(T)$ was defined at the commonly used criterion $R(T, H_{c2}) = 0.9R_n(T, H)$, where R_n is the normal-state resistance.

We chose this 90% criterion to extrapolate H_{c2} from resistive transitions to reduce the effect of thermal fluctuations and sample inhomogeneities on H_{c2} . Different resistive criteria may affect the measured $H_{c2}(T)$ temperature dependencies, as was shown for Nd-1111 pnictide single crystals.¹¹ Moreover, specific heat and transport measurements produce somewhat different results for H_{c2} .²⁶ This discrepancy may naturally result from the inevitable local T_c inhomogeneities, which determine the transition width even in the best chalcogenide single crystals.²⁶ Since the variations of T_c on scales greater than the coherence length result in a distribution of local H_{c2} , there is no unambiguous definition for the global H_{c2} in an inhomogeneous superconductor. As a result, transport and specific heat measurements probe different parts of the distribution of H_{c2} . Magnetotransport at the onset of superconductivity probes the higher- T_c part of the H_{c2} distribution in regions, which form a percolative cluster. The specific heat measurements probe both higher- T_c and lower- T_c parts of the H_{c2} distribution, which correspond to regions in which superconductivity could be modified by local nonstoichiometry or strains that cause deviation of the local Fe-As or Fe-(Te,Se) bond angles.^{2,3} Moreover the effect of thermal fluctuations can change the shape of resistivity and specific heat curves in different ways.

Figure 2 shows that the in-field transitions of Ba-1 taken in the 60-T magnet with a pulse width of ~ 75 ms are clean and sharp, indicating the high quality of our samples. The transition curves $R(H)$ obtained in the 85-T magnet are only slightly noisier because of the shorter pulse width (~ 15 ms). $H_{c2}^{||}(T)$ and $H_{c2}^{\perp}(T)$ are shown in Fig. 3(a) for the optimally doped and underdoped $\text{Ba}_{1-x}\text{K}_x\text{Fe}_2\text{As}_2$, where $//$ and \perp correspond

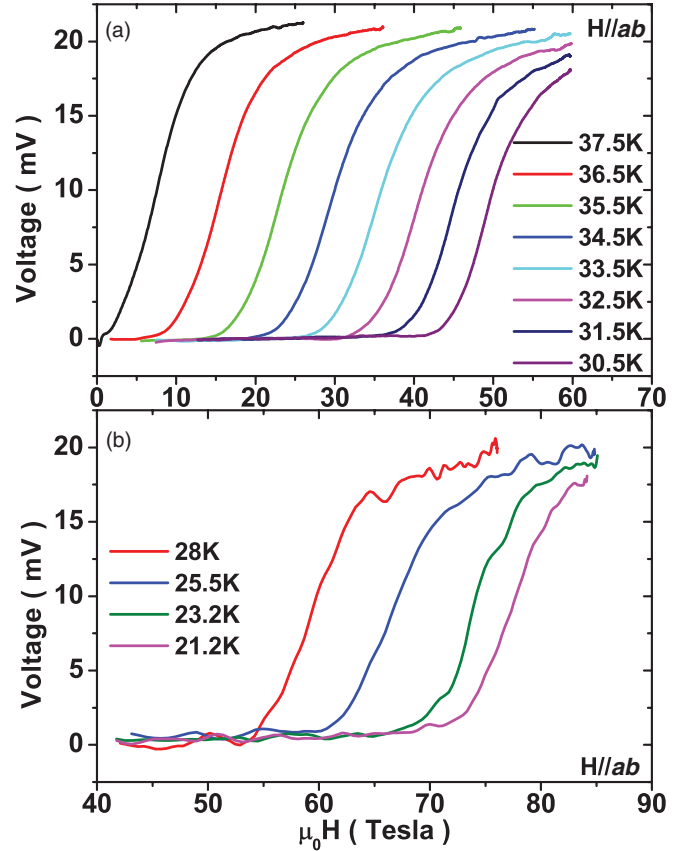


FIG. 2. (Color online) Superconducting transitions for Ba-1 in the (a) 60-T and (b) 85-T pulsed magnets.

to the magnetic fields parallel and perpendicular to the ab planes, respectively. Here, $H_{c2}^{||}(T)$ curves have downward curvatures in all cases. By contrast, $H_{c2}^{\perp}(T)$ for the optimally doped Ba-1 and slightly underdoped Ba-2 have downward curvatures, whereas $H_{c2}^{\perp}(T)$ for the most underdoped Ba-3 has an upward curvature. This behavior is consistent with the behavior of orbitally limited $H_{c2}(T)$ for a multiband s^{\pm} pairing, where the order parameter changes sign on different sheets of the FS.¹² As T decreases, the anisotropy parameter $\gamma(T) = H_{c2}^{||}(T)/H_{c2}^{\perp}(T)$ decreases from $\gamma(T_c) \approx 2$ to $\gamma(0) \approx 1$. Going from the strongly underdoped Ba-3 to the underdoped Ba-2 sample, $H_{c2}(T)$ nearly doubles, but $H_{c2}^{\perp}(T)$ flattens at low T and the upward curvature disappears. For the optimally doped Ba-1, $H_{c2}(0)$ is well above the 85-T limit of our measurements. Normalizing H_{c2} data to T_c , as shown in Fig. 3, reveals a similar trend for Ba-1 and Ba-2 but a clearly different behavior for Ba-3, showing that H_{c2} does not simply scale with T_c because the shape of $H_{c2}(T)$ changes upon doping.

Figure 4 shows the in-field resistive transitions in $\text{FeSe}_{0.5}\text{Te}_{0.5}$ film measured in the 60-T magnet. The comparatively sharp transitions at the highest magnetic field indicate good homogeneity of the sample. Figure 5 shows $H_{c2}(T)$ measured on $\text{FeSe}_{0.5}\text{Te}_{0.5}$ films, which all have $H_{c2}(T)$ with downward curvatures for both field orientations. In particular, $H_{c2}^{||}(T)$ has very steep slopes H_{c2}' near T_c , resulting in $H_{c2}^{||}(T_c/2) > 40$ T. Figure 5(c) shows an example of the

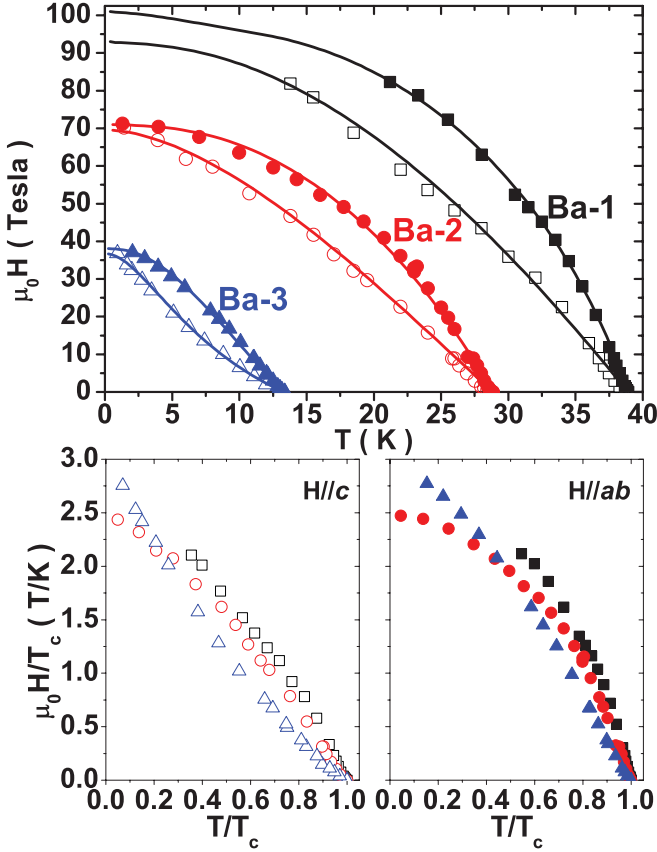


FIG. 3. (Color online) (a) $H_{c2}(T)$ curves for $\text{Ba}_{1-x}\text{K}_x\text{As}_2\text{Fe}_2$ single crystals with different doping levels ($H//ab$ and $H//c$ are full and empty symbols, respectively) and fits with the two-band theory (continuous lines). For Ba-1, $s = 1$, $\eta = 0.9$, $\alpha\varepsilon^{-1/2} = 1.9$ ($H//ab$) and $s = 1$, $\eta = 0.9$, $\alpha = 0.5$ ($H//c$). For Ba-2, $s = 1$, $\eta = 0.6$, $\alpha\varepsilon^{-1/2} = 0.8$ ($H//ab$) and $s = 1$, $\eta = 0.6$, $\alpha = 0.05$ ($H//c$). For Ba-3, $s = 1$, $\eta = 0.07$, $\alpha\varepsilon^{-1/2} = 0.14$ ($H//ab$) and $s = 1$, $\eta = 0.01$, $\alpha = 0.02$ ($H//c$). (b) and (c) data from (a) are normalized to T_c .

resistance curve $R(T)$ for one of the $\text{FeSe}_{0.5}\text{Te}_{0.5}$ films, which shifted by only 2mK at 1 T, corresponding to $H_{c2}' = 500$ T/K [Fig. 5(d)]. Such extremely high H_{c2} slopes near T_c are characteristic of our strained films, with H_{c2}' ranging from 250 to 500 T/K for $H//ab$ and from 8 to 21 T/K for $H//c$ (no apparent correlation between film thickness and H_{c2}' was found). For a different H_{c2} criterion (e.g., $R(T, H_{c2}) = 0.5R_n(T, H)$), the slope still exceeds 100 T/K, larger than any value previously reported in strain-free optimally doped $\text{FeSe}_{0.5}\text{Te}_{0.5}$ single crystals ($H_{c2}' = 13\text{--}40$ T/K).¹⁰

III. ANALYSIS OF THE EXPERIMENTAL DATA

We interpret our $H_{c2}(T)$ data using a model of $H_{c2}(T)$ that takes into account orbital and paramagnetic pair breaking and FFLO instability in clean multiband superconductors.¹² FFLO instability at $H = H_{c2}$ is characterized by the wave vector \mathbf{Q} of spatial oscillations of the superconducting order parameter $\Psi(\mathbf{r}) = \Delta(x, y)[c_1 \exp(iQz) + c_2 \exp(-iQz)]$, which appear spontaneously below the temperature T_F along \mathbf{H} (if \mathbf{H} is parallel to the symmetry axis). The equation for H_{c2}^\perp is given

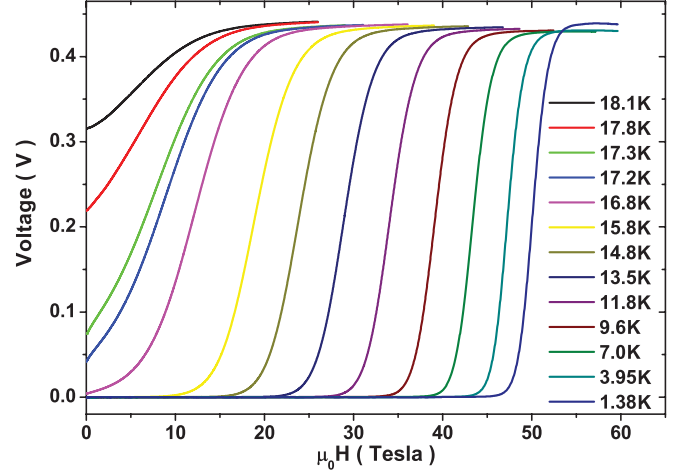


FIG. 4. (Color online) Superconducting transitions for a strained $\text{FeSe}_{1-x}\text{Te}_x$ thin film in high field.

by

$$a_1 G_1 + a_2 G_2 + G_1 G_2 = 0, \quad (1)$$

$$G_1 = \ln t + 2e^{q^2} \text{Re} \sum_{n=0}^{\infty} \int_q^{\infty} e^{-u^2} \left[\frac{u}{n+1/2} - \frac{t}{\sqrt{b}} \tan^{-1} \left(\frac{u\sqrt{b}}{t(n+1/2) + i\alpha b} \right) \right] du, \quad (2)$$

where G_2 is obtained by substituting $\sqrt{b} \rightarrow \sqrt{\eta b}$ and $q \rightarrow q\sqrt{s}$ in G_1 . Here, $Q(T, H)$ is determined by the condition that $H_{c2}(T, Q)$ is maximum, $a_1 = (\lambda_0 + \lambda_-)/2w$, $a_2 = (\lambda_0 - \lambda_-)/2w$, $\lambda_- = \lambda_{11} - \lambda_{22}$, $\lambda_0 = (\lambda_-^2 + 4\lambda_{12}\lambda_{21})^{1/2}$, $w = \lambda_{11}\lambda_{22} - \lambda_{12}\lambda_{21}$, $t = T/T_c$, and

$$b = \frac{\hbar^2 v_1^2 H}{8\pi \phi_0 k_B^2 T_c^2}, \quad q^2 = \frac{Q_c^2 \varepsilon_1 \phi_0}{2\pi H}, \quad \alpha = \frac{4\mu \phi_0 T_c}{\hbar^2 v_1^2}, \quad (3)$$

where $\eta = (v_2/v_1)^2$, $s = \varepsilon_2/\varepsilon_1$, v_i is the in-plane Fermi velocity in band $i = 1, 2$, $\varepsilon_i = m_i^{ab}/m_i^c$ is the mass anisotropy ratio, ϕ_0 is the flux quantum, μ is the magnetic moment of a quasiparticle, λ_{11} and λ_{22} are the intraband pairing constants, λ_{12} and λ_{21} are the interband pairing constants, and $\alpha \approx \alpha_M/1.8$, where the Maki parameter $\alpha_M = 2^{1/2} H_{c2}^{\text{orb}}/H_p$ quantifies the strength of the Zeeman pair breaking. The fits for $H//ab$ were done assuming that the bands have the same anisotropy parameter $\varepsilon_1 = \varepsilon_2 = \varepsilon$ for which H_{c2}^{\perp} is defined by Eqs. (1)–(3) with the rescaled $q \rightarrow q\varepsilon^{-3/4}$, $\alpha \rightarrow \alpha\varepsilon^{-1/2}$, and $b^{1/2} \rightarrow b^{1/2}\varepsilon^{1/4}$ in G_1 and $(\eta b)^{1/2} \rightarrow (\eta b)^{1/2}\varepsilon^{1/4}$ in G_2 .¹²

Figures 3 and 5 show the fits of this theory to the data, where the shape of $H_{c2}(T)$ is determined by the ratio of the in-plane Fermi velocities $\eta = (v_2/v_1)^2$ for bands 1 and 2, the mass anisotropy ratio $\varepsilon = m_{ab}/m_c$, and the Pauli pair-breaking parameter $\alpha = \pi k_B T_c m_{ab}/E_F m_e$ (m_{ab} is the electron effective mass in the ab plane, m_e is the free electron mass $E_F = m_{ab} v_1^2/2$, and bands 1 and 2 correspond to the hole and electron pockets of the FS, respectively). In a single-band superconductor, the condition $\alpha \geq 1$ means that Pauli pair breaking significantly changes the shape of $H_{c2}(T)$, resulting in FFLO instability. As shown in Fig. 3, the upward curvature

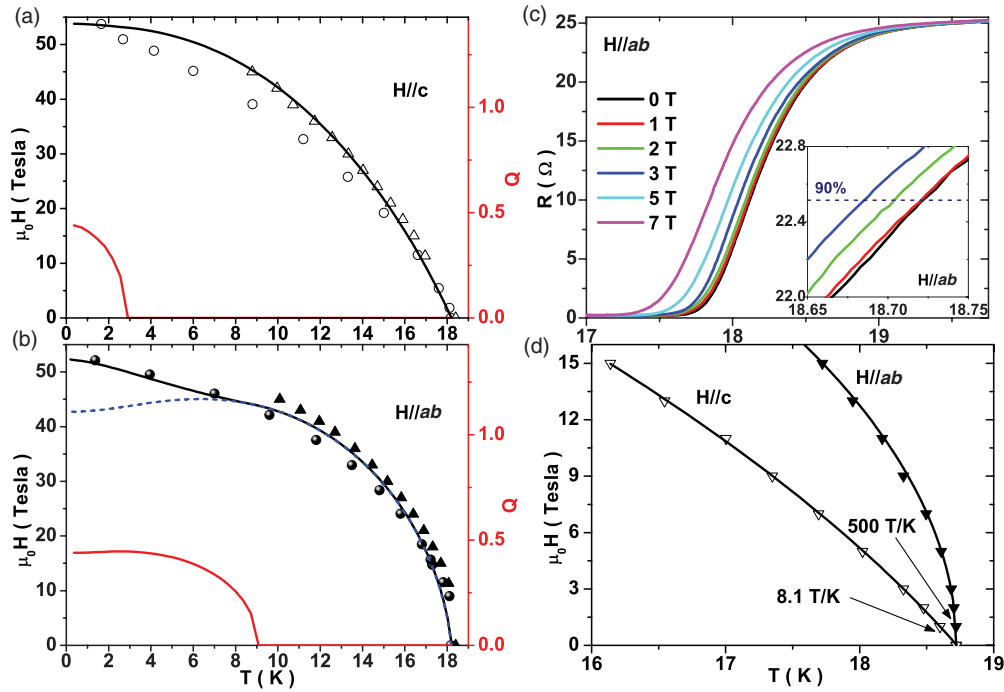


FIG. 5. (Color online) (a) and (b) $H_{c2}(T)$ curves for two strained $\text{FeSe}_{1-x}\text{Te}_x$ thin films with similar T_c measured in the 45-T DC magnet (triangles) and in the 60-T pulsed magnet (circles) (full and empty symbols represent $H//ab$ and $H//c$, respectively). The black solid curves correspond to H_{c2} fits, and the red solid curves correspond to the \mathbf{Q} vector of the FFLO state. The blue dashed line in (b) shows $H_{c2}(T)$ calculated without taking FFLO instability into account. Fit parameters are $\alpha = 1.2$ and $\eta = 0.9$ for $H//c$ and $\alpha\varepsilon^{-1/2} = 7$ for $H//ab$. Here, Q is measured in the units of $Q_0 = 4\pi k_B T_c / \hbar v_1 \varepsilon^{3/4}$. (c) Superconducting transitions at low fields ($H//ab$) of a $\text{FeSe}_{1-x}\text{Te}_x$ film and a magnification close to 90% of the normal state resistivity. (d) For the same sample, the detailed H_{c2} data close to T_c show the extremely high slope for $H//ab$. Here, the continuous lines show $H_{c2}(T) \propto (T_c - T)^{1/2}$, indicating complete suppression of orbital pair breaking.

of $H_{c2}^{\perp}(T)$ for strongly underdoped Ba-3 corresponds to the s^{\pm} pairing for $\eta = 0.01$ and $\alpha = 0.02$. Here, paramagnetic effects are negligible in band 1, where $\alpha_1 \approx \alpha \ll 1$, but are essential in band 2, where $\alpha_2 \approx \alpha/\eta = 2$. For $H//ab$, the change in the curvature of $H_{c2}^{\parallel}(T)$ in Fig. 3 is attributed to strong mass anisotropy $\varepsilon \approx 0.02$, which increases $\alpha \rightarrow \alpha\varepsilon^{-1/2}$ and flattens $H_{c2}^{\parallel}(T)$ at low T . For Ba-1 and Ba-2, $H_{c2}^{\perp}(T)$ can be described assuming a moderate band asymmetry for the parameters given in the Fig. 3 caption. The fitting curves $H_{c2}(T)$ for the optimally doped Ba-1 at low temperatures extrapolate to ~ 100 T above the upper limit of our high-field measurements. The fits suggest the appearance of the FFLO state below 10K for the optimally doped Ba-1 sample at $H//ab$.

The shapes of $H_{c2}(T)$ for $\text{FeSe}_{1-x}\text{Te}_x$ films shown in Fig. 5 indicate strong Pauli pair breaking consistent with the previous measurements.^{8,10} The fits correspond to $\alpha_{\perp} = 1.2$ for $H \perp ab$ and $\alpha_{\parallel} = \alpha_{\perp} \varepsilon^{-1/2} = 7$ and $\varepsilon \approx 0.03$ for $H//ab$, for which theory suggests FFLO instability below 3K–9K, where the FFLO wave vector $\mathbf{Q}(T)$ appears spontaneously, as shown in Fig. 5. The principal importance of FFLO instability for the interpretation of our experimental data is particularly evident in the case of $H//ab$. Here, $H_{c2}(T)$ calculated without FFLO instability (dashed line in Fig. 5) is inconsistent with the observed $H_{c2}(T)$, which exhibits a very steep rise near T_c , indicative of $\alpha \gg 1$ and a nearly linear temperature dependence at low T . By contrast, taking FFLO instability into account in Eqs. (1)–(3) enables us to explain the shapes of the $H_{c2}^{\parallel}(T)$ curves observed on our $\text{FeSe}_{1-x}\text{Te}_x$ films, as

shown in Fig. 5 (solid line). The conclusion about strong Pauli pair breaking and FFLO instability at $H//ab$ is consistent with the parameters of $\text{FeSe}_{1-x}\text{Te}_x$ extracted from ARPES,²⁷ which yields $E_F \approx 20$ –30 meV and $m_{ab}/m_e = 3$ –16 for different FS pockets, giving $\alpha \approx 0.5$ –4 for $H \perp ab$. Next we use the orbitally limited slope H_{c2}' near T_c in the two-band model¹²

$$H_{c2}' = \frac{24\pi k_B^2 T_c \phi_0}{7\zeta(3)\hbar^2 (c_1 v_1^2 + c_2 v_2^2)}, \quad (4)$$

where $\zeta(3) = 1.202$ and c_1 and c_2 depend on inter- and intraband coupling constants.¹² For the s^{\pm} model in which interband pairing dominates, $c_1 \rightarrow c_2 \rightarrow 1/2$ and Eq. (3) yields $H_{c2}' [\text{T/K}] = 1.8 T_c [\text{K}] m_{ab} / \{m_e (1+\eta) E_{F1} [\text{meV}]\}$. The observed slope $H_{c2}' \approx 8$ T/K corresponds to $m_{ab}/m_e \approx 12$ for $T_c = 18$ K, $E_F = 25$ meV, and $\eta = 1$ or $m_{ab}/m_e \approx 6$ if $\eta \ll 1$. Again, these values of m_{ab}/m_e are qualitatively consistent with the ARPES data.²⁷ Small E_F and large m_{ab} in $\text{FeSe}_{1-x}\text{Te}_x$ thus yield $\alpha > 1$ even for $H//c$, so the FFLO state for $H//ab$ is a realistic possibility that may be explicitly verified by magnetic torque, specific heat, or nuclear magnetic resonance (NMR) measurements. The very short Ginzburg-Landau (GL) coherence lengths $\xi_{ab} = (\phi_0/2\pi T_c H_{c2}')^{1/2} \approx 1.5$ nm for $H_{c2}' = 8.1$ T/K ($H \perp ab$) and $\xi_c = \xi_{ab} H_{c2}'^{\parallel}/H_{c2}^{\perp} < 0.12$ nm for $H_{c2}' > 100$ T/K ($H//ab$) extracted from the data in Fig. 5 show that our $\text{FeSe}_{1-x}\text{Te}_x$ films are indeed in the clean limit.

The multiband structure of FBSs allows tuning of $H_{c2}(T)$ by small shifts of the Fermi level, which changes the Fermi velocities and can open small FS pockets that enhance

Pauli pair breaking.¹² For instance, $\text{Ba}_{1-x}\text{K}_x\text{Fe}_2\text{As}_2$ has two- or three-hole FS pockets and two-electron FS pockets.^{17–20} In particular, as shown in ARPES experiments,^{19,20} in the underdoped cases there is a hole band at Γ below the Fermi level, but at optimal doping this band emerges and crosses the Fermi level. So doping changes the ratio of the Fermi velocities $\eta = (v_2/v_1)^2$ and the intraband parameters α , which in turn changes the shape of $H_{c2}(T)$ in Fig. 3. The α parameter for Ba-1 is significantly larger than that for the two underdoped samples (0.5 vs 0.02–0.05), so the effect of Pauli pair breaking on the shape of $H_{c2}(T)$ curves in Ba-122 remains relatively moderate, unlike the more Pauli-limiting case of $\text{FeSe}_{1-x}\text{Te}_x$.

An interesting situation occurs in $\text{FeSe}_{1-x}\text{Te}_x$, which has two-hole FS pockets at the Γ point of the Brillouin zone and a hole band just slightly below the Fermi level at $x = 0.58$.^{27–29} This band structure allows us to use the following model¹² of the extremely high H_{c2} slopes in our strained $\text{FeSe}_{1-x}\text{Te}_x$ films. As x is changed from 0.58 ($T_c = 11.5\text{K}$)²⁷ to 0.5, T_c climbs to 16K (18K under strain) and a new hole FS pocket emerges, while the electron FS pocket at M shrinks. This emerging hole pocket, driven either by doping or by strain, has a small Fermi energy E_F and strongly enhanced effective mass m_{ab} ^{27,29,30} and thus a large Pauli pair-breaking parameter $\alpha \propto m_{ab}/E_F$, which reduces the role of orbital pair breaking for the other hole FS pockets at the Γ point, thus increasing the slopes of H_{c2} at T_c .¹² Consistent with this model, the large substrate-induced compressive strain of our films shows much higher H_{c2} slopes than previous measurements on $\text{FeSe}_{1-x}\text{Te}_x$ single crystals^{8–10} and huge slopes for $H//ab$. The emerging hole FS pocket can further reduce the small c -axis GL coherence length $\xi_c \approx 0.12$ nm, which is already less than half the spacing $c = 0.55$ nm between the ab planes² for $H_{c2}' > 100$ T/K for $H//ab$ shown in Fig. 5. The slopes $H_{c2}' > 100$ T/K in our strained films are consistent with the collapse of ξ_c triggered by the opening of the hole FS pocket, which decouples the ab planes and results in a dimensional crossover³¹ $\xi_c(T) < 2^{-1/2}c$ at $T = T^*$ very close to T_c . For $T < T^*$, $H_{c2}'(T)$ is mostly limited by Pauli pair breaking for which $H_{c2}'(T) \propto (T^* - T)^{1/2}$, where T^* is very close to T_c . So the slope H_{c2}' at T_c is enhanced by the large factor $\approx [T_c/(T_c - T^*)]^{1/2}$ with respect to the orbital limit. Indeed, $H_{c2}'(T) \propto (T_c - T)^{1/2}$ describes well our experimental data on the films with the highest H_{c2} slopes near T_c , as displayed in Fig. 5(d).

IV. DISCUSSION

To demonstrate how much H_{c2} can be enhanced by doping and strain, we compare our optimally doped Ba-1 crystal and $\text{FeSe}_{1-x}\text{Te}_x$ films with other superconductors. Figure 6 shows that $H_{c2}(0)$ for $\text{FeSe}_{1-x}\text{Te}_x$ is almost twice as high as for Nb_3Sn , despite their same $T_c = 18\text{K}$. Yet the Pauli-limited $H_{c2}(0)$ of $\text{FeSe}_{1-x}\text{Te}_x$ is lower than the $H_{c2}(0)$ of PbMo_6S_8 ,³² which has $T_c = 14\text{K}$ and the orbitally limited shape of $H_{c2}(T)$,¹⁶ likely due to larger E_F and smaller α . Our $\text{Ba}_{0.6}\text{K}_{0.4}\text{Fe}_2\text{As}_2$ single crystal has much higher $H_{c2}(T)$ than $\text{Ba}_{0.55}\text{K}_{0.45}\text{Fe}_2\text{As}_2$ ⁴ and $\text{Ba}_{0.68}\text{K}_{0.32}\text{Fe}_2\text{As}_2$,²¹ whereas below 36K, $\text{Ba}_{0.6}\text{K}_{0.4}\text{Fe}_2\text{As}_2$ surpasses $\text{NdFeAsO}_{1-x}\text{F}_x$ ¹¹ despite its higher T_c . The latter indicates that $H_{c2}(T)$ in FBSs do not

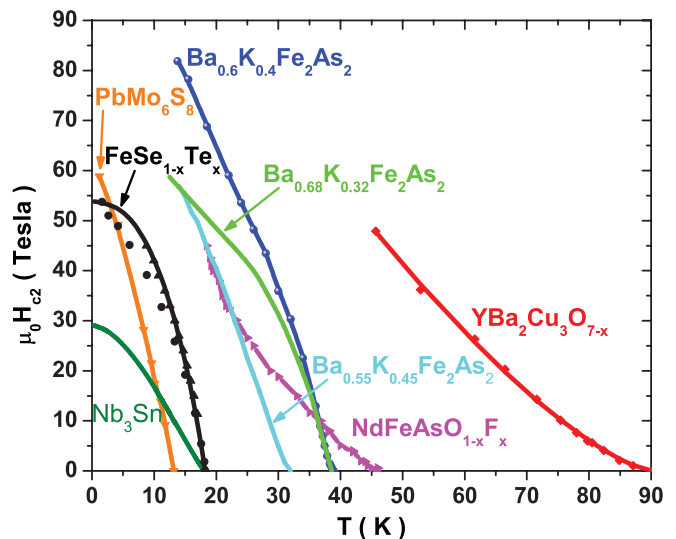


FIG. 6. (Color online) Comparison of the upper critical fields of different materials: $H_{c2}(T)$ data of Nb_3Sn , PbMo_6S_8 (Ref. 32), $\text{FeSe}_{1-x}\text{Te}_x$ (this paper), $\text{Ba}_{0.55}\text{K}_{0.45}\text{Fe}_2\text{As}_2$ (Ref. 4), $\text{Ba}_{0.68}\text{K}_{0.32}\text{Fe}_2\text{As}_2$ (Ref. 21), $\text{Ba}_{0.6}\text{K}_{0.4}\text{Fe}_2\text{As}_2$ (this paper), $\text{NdFeAsO}_{1-x}\text{F}_x$ (Ref. 11), and the irreversibility field of $\text{YBa}_2\text{Cu}_3\text{O}_{7-x}$.

simply scale with T_c , since the multiband effects and the interplay of orbital and Pauli pair breaking can result in more complex and interesting behavior.

Our high-field measurements have shown that the observed shape of $H_{c2}(T)$ curves for $H//ab$ in chalcogenide films is inconsistent with the conventional Werthamer-Helfand-Hohenberg-based multiband theory^{12,16} if FFLO instability is disregarded, but it can be explained by taking into account the FFLO state at low temperatures. We hope that this result may motivate other experimental groups to verify it by independent NMR, magnetic torque, or specific heat measurements. However, the two latter techniques may not unambiguously reveal the FFLO state if the weak features of the first-order FFLO transition¹⁵ are smeared by T_c inhomogeneities characteristic of even the best chalcogenide single crystals.²⁶

V. CONCLUSIONS

Our high-field measurements show quite explicitly how the behavior of $H_{c2}(T)$ in $\text{Ba}_{1-x}\text{K}_x\text{As}_2\text{Fe}_2$ can be effectively tuned by doping, resulting in $H_{c2} \approx 85$ T at $\sim T_c/2$. Our strained $\text{FeSe}_{1-x}\text{Te}_x$ films exhibit an extreme Pauli-limited $H_{c2}(T)$, indicative of the FFLO state. The observed suppression of orbital pair breaking causes significant enhancement of H_{c2} of the optimally doped $\text{Ba}_{1-x}\text{K}_x\text{As}_2\text{Fe}_2$ (at low temperature more than 25 T larger than the previous results^{4,21} on both slightly underdoped and overdoped $\text{Ba}_{1-x}\text{K}_x\text{As}_2\text{Fe}_2$), which could make Ba-122 a competitive high-field magnet material.

ACKNOWLEDGMENTS

A portion of this work was performed at the National High Magnetic Field Laboratory, which is supported by US Natural Science Foundation Cooperative Agreement

No. DMR-0654118, by the State of Florida, and by the US Department of Energy. The work in Beijing is supported partly by the Ministry of Science and Technology of China

(973 Project No. 2011CBA01000) and the Natural Science Foundation of China. We are grateful to M. Jaime, J. Betts, and M. Putti for discussion and experimental help.

*tarantini@asc.magnet.fsu.edu

- ¹Y. Kamihara, T. Watanabe, M. Hirano, and H. Hosono, *J. Am. Chem. Soc.* **130**, 3296 (2008).
- ²D. C. Johnston, *Adv. Phys.* **59**, 803 (2010).
- ³J. Paglione and R. L. Greene, *Nat. Phys.* **6**, 645 (2010).
- ⁴M. M. Altarawneh, K. Collar, C. H. Mielke, N. Ni, S. L. Budko, and P. C. Canfield, *Phys. Rev. B* **78**, 220505(R) (2008).
- ⁵G. Fuchs *et al.*, *New J. Phys.* **11**, 075007 (2009).
- ⁶A. Yamamoto *et al.*, *Appl. Phys. Lett.* **94**, 062511 (2009).
- ⁷H. Q. Yuan, J. Singleton, F. F. Balakirev, S. A. Baily, G. F. Chen, J. L. Luo, and N. L. Wang, *Nature* **457**, 565 (2009).
- ⁸M. Fang, J. Yang, F. F. Balakirev, Y. Kohama, J. Singleton, B. Qian, Z. Q. Mao, H. Wang, and H. Q. Yuan, *Phys. Rev. B* **81**, 020509(R) (2010).
- ⁹T. Kida, T. Matsunaga, M. Hagiwara, Y. Mizuguchi, Y. Takano, and K. Kindo, *J. Phys. Soc. Jpn.* **78**, 113701 (2009).
- ¹⁰T. Klein *et al.*, *Phys. Rev. B* **82**, 184506 (2010).
- ¹¹J. Jaroszynski *et al.*, *Phys. Rev. B* **78**, 174523 (2008).
- ¹²A. Gurevich, *Phys. Rev. B* **82**, 184504 (2010); A. Gurevich, *Rep. Prog. Phys.* **74**, 124501 (2011).
- ¹³P. Fulde and R. A. Ferrel, *Phys. Rev.* **135**, A550 (1964).
- ¹⁴A. I. Larkin and Y. N. Ovchinnikov, *Zh. Eksp. Teor. Fiz.* **47**, 1136 (1964) [*Sov. Phys. JETP* **20**, 762 (1965)].
- ¹⁵Y. Matsuda and H. Shimahara, *J. Phys. Soc. Jpn.* **76**, 051005 (2007).
- ¹⁶N. R. Werthamer, E. Helfand, and P. C. Hohenberg, *Phys. Rev.* **147**, 295 (1966).
- ¹⁷H. Ding *et al.*, *Eur. Phys. Lett.* **83**, 47001 (2008).
- ¹⁸M. Yi *et al.*, *Phys. Rev. B* **80**, 024515 (2009).
- ¹⁹H. Ding *et al.*, *J. Phys. Condens. Matter* **23**, 135701 (2011).
- ²⁰M. Neupane *et al.*, *Phys. Rev. B* **83**, 094522 (2011).
- ²¹V. A. Gasparov, F. Wolff-Fabris, D. L. Sun, C. T. Lin, and J. Wosnitzer, *JETP Lett.* **93**, 26 (2001).
- ²²H. Q. Luo, Z. Wang, H. Yang, P. Cheng, X. Zhu, and H. H. Wen, *Supercond. Sci. Technol.* **21**, 125014 (2008).
- ²³G. Mu, H. Luo, Z. Wang, L. Shan, C. Ren, and H. H. Wen, *Phys. Rev. B* **79**, 174501 (2009).
- ²⁴E. Bellingeri, R. Buzio, A. Gerbi, D. Marrè, S. Congiu, M. R. Cimberle, M. Tropeano, A. S. Siri, A. Palenzona, and C. Ferdeghini, *Supercond. Sci. Technol.* **22**, 105007 (2009).
- ²⁵E. Bellingeri, I. Pallecchi, R. Buzio, A. Gerbi, D. Marrè, M. R. Cimberle, M. Tropeano, M. Putti, A. Palenzona, and C. Ferdeghini, *Appl. Phys. Lett.* **96**, 102512 (2010).
- ²⁶A. Serafin, A. I. Coldea, A. Y. Ganin, M. J. Rosseinsky, K. Prassides, D. Vignolles, and A. Carrington, *Phys. Rev. B* **82**, 104514, (2010).
- ²⁷A. Tamai *et al.*, *Phys. Rev. Lett.* **104**, 097002 (2010).
- ²⁸F. Chen *et al.*, *Phys. Rev. B* **81**, 014526 (2010).
- ²⁹K. Nakayama *et al.*, *Phys. Rev. Lett.* **105**, 197001 (2010).
- ³⁰H. Shishido *et al.*, *Phys. Rev. Lett.* **104**, 057008 (2010).
- ³¹R. A. Klemm, A. Luther, and M. R. Beasley, *Phys. Rev. B* **12**, 877 (1975).
- ³²K. Okuda, M. Kitagawa, T. Sakakibara, and M. Date, *J. Phys. Soc. Jpn.* **48**, 2157 (1980).